Journal of Energy Storage 177 (2026) 123425

Contents lists available at ScienceDirect

Journal of Energy Storage

journal homepage: www.elsevier.com/locate/est

Research papers

Novel Ethylene-Propylene-Diene Monomer rubber panels filled with Phase Change Material and expanded graphite for energy efficiency of buildings

Sereno Sacchet [a,*], Alessandro Pizzato [a], Francesco Valentini [a], Maurizio Grigiante [b], Riccardo Po [c], Luca Fambri [a,*]

[a] Department of Industrial Engineering and INSTM Research Unit, University of Trento, 38123, Italy
[b] Department of Civil, Environmental and Mechanical Engineering, University of Trento, 38123, Trento, Italy
[c] Renewable, New Energies and Materials Science Research Center, "Istituto Guido Donegani", Eni S.p.A., 28100, Novara, Italy

ARTICLE INFO

Keywords:
Thermal management
PCM
EPDM rubber
Composite Mechanical Modelling
Expanded Graphite

ABSTRACT

The integration of organic Phase Change Materials (PCMs) in building walls has become essential to surpassing the limitations of conventional insulation. Within this scope, we developed novel Ethylene-Propylene-Diene Monomer (EPDM) composite materials incorporating paraffin as PCM. To achieve this, Expanded Graphite (EG) was introduced via a preliminary vacuum impregnation process. This carbonaceous filler acts as a multi-functional support, ensuring shape stability and enhancing the structural integrity of the rubber matrix. The resulting composites exhibit an outstanding melting enthalpy of 167 J/g—a record-high value for EPDM-based systems within the 22–31 °C range—while the percolative EG network raises thermal conductivity to 1.7 W/m·K (a ten-fold increase over the neat PCM). Dynamic thermal tests in a climatic chamber confirmed a significant thermal lag and the ability to dampen temperature peaks effectively. Furthermore, mechanical characterization at 21 °C and 40 °C demonstrated that the panels maintain a compressive strength exceeding 0.1 MPa even when the PCM is molten, ensuring structural reliability during storage and transport. In summary, leveraging a superior synergy between heat storage and thermal transport validated by Figure of Merit (FoM) analysis, these novel PCM/EG-based panels offer a high-performance solution for passive cooling applications in sustainable architecture.

1. Introduction

Currently, the building sector is one of the primary contributors to energy consumption in Europe, accounting for approximately 27% of the EU's total energy use [1,2]. Notably, 85% of EU buildings were constructed before 2001, and the majority exhibit poor energy performance [3,4]. Enhancing building energy efficiency is therefore critical for reducing energy waste, lowering utility costs for individuals and small businesses, and achieving a zero-emission building stock by 2050, in alignment with the European Green Deal [2]. Furthermore, improving thermal performance of buildings serves to alleviate energy poverty and strengthen Europe's energy independence. Meeting these objectives requires a dual strategy: reducing energy demand through optimized insulation of inefficient structures [5], and developing advanced building systems that integrate technologies for thermal energy transfer and storage to attenuate peak loads and optimize energy use over time [6–8].

Phase Change Materials (PCMs) have been extensively researched for their ability to absorb and release significant latent heat during phase transitions, a characteristic that makes them ideal for thermal regulation applications [9–14]. Generally, PCM applications are categorized into two primary fields: Thermal Energy Storage (TES) and Thermal Energy Management (TEM). In TES, PCMs store heat over extended periods to reduce cumulative energy demand and shift peak loads [15–17]. Conversely, in TEM, PCMs function as thermal buffers to mitigate temperature spikes in systems subjected to high thermal fluxes, such as electronic components, battery arrays, or building envelopes exposed to fluctuating solar radiation [18–22].

Over the past two decades, TEM has emerged as a vital research area for improving energy efficiency in civil applications. Among the various types of PCMs, fatty acids and paraffin waxes are frequently utilized in building applications due to their favourable thermal properties, chemical stability, and phase-change temperatures that align with indoor comfort requirements [23–25]. Despite these advantages, their

* Corresponding authors.
E-mail addresses: sereno.sacchet@unitn.it (S. Sacchet), luca.fambri@unitn.it (L. Fambri).

https://doi.org/10.1016/j.est.2026.123425
Received 7 February 2026; Received in revised form 5 June 2026; Accepted 4 July 2026
Available online 10 July 2026

practical implementation is often hindered by low thermal conductivity [26–28] and the risk of leakage during phase transitions [29–34]. To be effectively integrated into building envelopes, PCMs must be stabilized to ensure structural compatibility and containment. Numerous studies have confirmed that embedding stabilized PCMs within walls or floors can effectively dampen indoor temperature fluctuations, shift peak heating and cooling loads, and significantly enhance occupant thermal comfort [35–41].

To address these limitations, PCMs are often incorporated into porous support matrices to create shape-stabilized composite PCMs. A notable advancement involves the double shape stabilization of PCMs within a porous support, like organ-modified montmorillonite (oMMT), and an elastomeric phase, like an ethylene-propylene diene monomer (EPDM) rubber matrix, selected for its flexibility, durability, and easy processing into panels [28,42]. This material has been successfully implemented for building temperature regulation by cladding walls with EPDM-based heat-absorbing panels, which demonstrated exceptional efficacy under summer conditions [43]. An alternative strategy involves embedding PCMs into high-conductivity carbon-based scaffolds [44]. Expanded graphite (EG), in particular, offers exceptionally high thermal conductivity along its basal planes [10]. Previous research demonstrated that incorporating 14 wt% EG into a stearic/palmitic acid PCM increased the thermal conductivity from 0.2 to 8.3 W/(m·K), —a 40-fold improvement—while the latent heat decreased only marginally from 196 to 169 J/g [45]. Moreover, EG contributes to the physical stabilization of the PCM by absorbing it into its porous structure, where the PCM remains confined even in the liquid state because of capillary forces. This mechanism prevents leakage during the phase transition while simultaneously establishing continuous thermal pathways that enhance the overall conductivity of the composite [46,47]. Within these form-stable composites, EG serves as a lightweight structure, percolating through the PCM molecules to establish a continuous thermal conductive network.

Moving beyond rigid carbonaceous scaffolds, recent literature has begun exploring the integration of these conductive networks directly into elastomeric matrices, mirroring the multi-phase stabilization approach. However, these recent advancements have been exclusively tailored for high-temperature industrial applications. For instance, Chen et al. [48] developed an EPDM/PCM/EG composite exhibiting a latent heat of 140 J/g under compressive loading-unloading cycles, but the melting temperature was restricted to the 40–50 °C range, making it unsuitable for ambient indoor comfort and instead targeting battery thermal management. Similarly, Shi et al. [49] incorporated exfoliated graphene nanoplatelets (GNP) into an EPDM/PCM system, achieving thermal conductivities up to 1.46 W/(m·K) but operating strictly within a high-temperature photovoltaic cooling window (40–65 °C). To address other harsh industrial environments, such as oil-immersed transformers, a flexible nitrile butadiene rubber (NBR)/PCM/oMMT composite was fabricated by Chen et al. [50], which suffered from lack of thermal conductivity data and operated at excessive temperatures (60–75 °C), far beyond the scope of civil engineering envelopes.

While these recent works demonstrate the thermal and structural potential of combining conductive carbon fillers with elastomeric blends, their integration into flexible EPDM matrices for ambient-temperature building applications remains an unaddressed gap in literature. Consequently, the aim of this study is replacing oMMT with EG to simultaneously overcome the low thermal conductivity of clay-based supports and the extreme operational temperatures of recent carbon-elastomer blends. This facilitates higher PCM loading and enhanced heat transfer specifically tailored for the human comfort temperature range of 20–30 °C. A commercial paraffin with a melting point of 28 °C was used as the PCM and vacuum-impregnated into EG. These components were then blended in various weight ratios with an elastomeric EPDM matrix to produce composite panels with tailored properties. The primary objective was to develop panels capable of providing the highest possible thermal management ability by maximizing their melting enthalpy. Following a preliminary study to determine the ideal composition, a comprehensive thermophysical and mechanical characterization was conducted on the prepared panels, accompanied by theoretical modelling of the composite stiffness. The produced PCM/EG rubber panels are compared in the final section using a Figure of Merit (FoM), which summarizes the main findings and benchmarks them against available literature research regarding the use of PCMs in different temperature ranges. Hence, this study aims to bridge the gap between high-capacity thermal storage and structural reliability, providing a scalable solution for energy-efficient building envelopes.

2. Experimental part

2.1. Materials

The organic PCM selected for the action of thermal regulation of building is RT28HC (RT28), a paraffin provided by Rubitherm GmbH (Berlin, Germany). It was characterized by melting enthalpy of 250 J/g and melting peak in the range 27–29 °C.

The Expanded Graphite (EG) used as conductive and structural filler was “SIGRAFLEX® Highly Conductive Expanded Graphite Powder”, provided by SGL Carbon GmbH (Meitingen, Germany), characterized by tapped density of 25 g/L at room temperature.

Vistalon® 2504 EPDM rubber is an amorphous terpolymer with low Mooney viscosity (ML 1 + 4, 125 °C) of 25 MU, medium diene content (4.7 wt% of ethylidene norbornene), and low ethylene content (58 wt %); it was supplied by Exxon Mobil (Irving, TX, USA). Zinc oxide (curing activator), stearic acid (curing activator and lubricating agent), and sulfur (vulcanizing agent) were supplied by Rhein Chemie (Cologne, Germany). The accelerants, tetramethylthiuram disulphide (TMTD) and zinc dibutyl dithiocarbamate (ZDBC) were obtained from Vibiplast srl (Castano Primo, Milan, Italy). Carbon black (N550), supplied by the Omsk Carbon Group (Omsk, Russia), was used as a reinforcing filler.

Nitrile-butadiene rubber (NBR) foils (thickness equal to 0.4 mm), with high acrylonitrile content (45 wt%), were purchased on the market. The NBR foils contained around 33 wt% of inorganic fillers in their composition, i.e. talc (11 wt%), kaolin (11 wt%), and silica (11 wt%).

2.2. Sample preparation

The samples were prepared in successive stages, beginning with the vacuum impregnation of the PCM into the EG. This initial shape-stabilization step was performed directly within a rotavapor (Fig. 1a), following procedures established in previous research [45,46]. Initially, the solid PCM and EG fillers were charged into a flask and subjected to a brief manual blending to ensure initial macroscopic distribution. The system was then connected to a rotary evaporator (Fig. 1a). While maintaining a constant rotation speed of 20 rpm, a vacuum of 10 mbar was applied at room temperature. This step was specifically designed to thoroughly evacuate air from the porous network of the EG prior to PCM infiltration, while the organic phase remained entirely in the solid state during this preliminary evacuation phase. Subsequently, the water bath was heated to approximately 90 °C, and the apparatus was maintained under vacuum for 30 min to ensure the molten PCM fully infiltrated the EG matrix. Continuous rotation was strictly maintained throughout this thermal step to guarantee a highly homogeneous impregnation. Following the infiltration period, the rotation was stopped, the vacuum was broken, and the flask was detached from the rotary evaporator. The mixture was then allowed to cool ambiently to room temperature, yielding a stable powder in which the PCM was successfully shape-stabilized. Three PCM/EG formulations were prepared by varying the EG content, expressed in parts per hundred ratio (phr). The respective sample codes and compositions for each formulation are listed in Table 1.

The neat EPDM compound was prepared by mixing the ingredients in

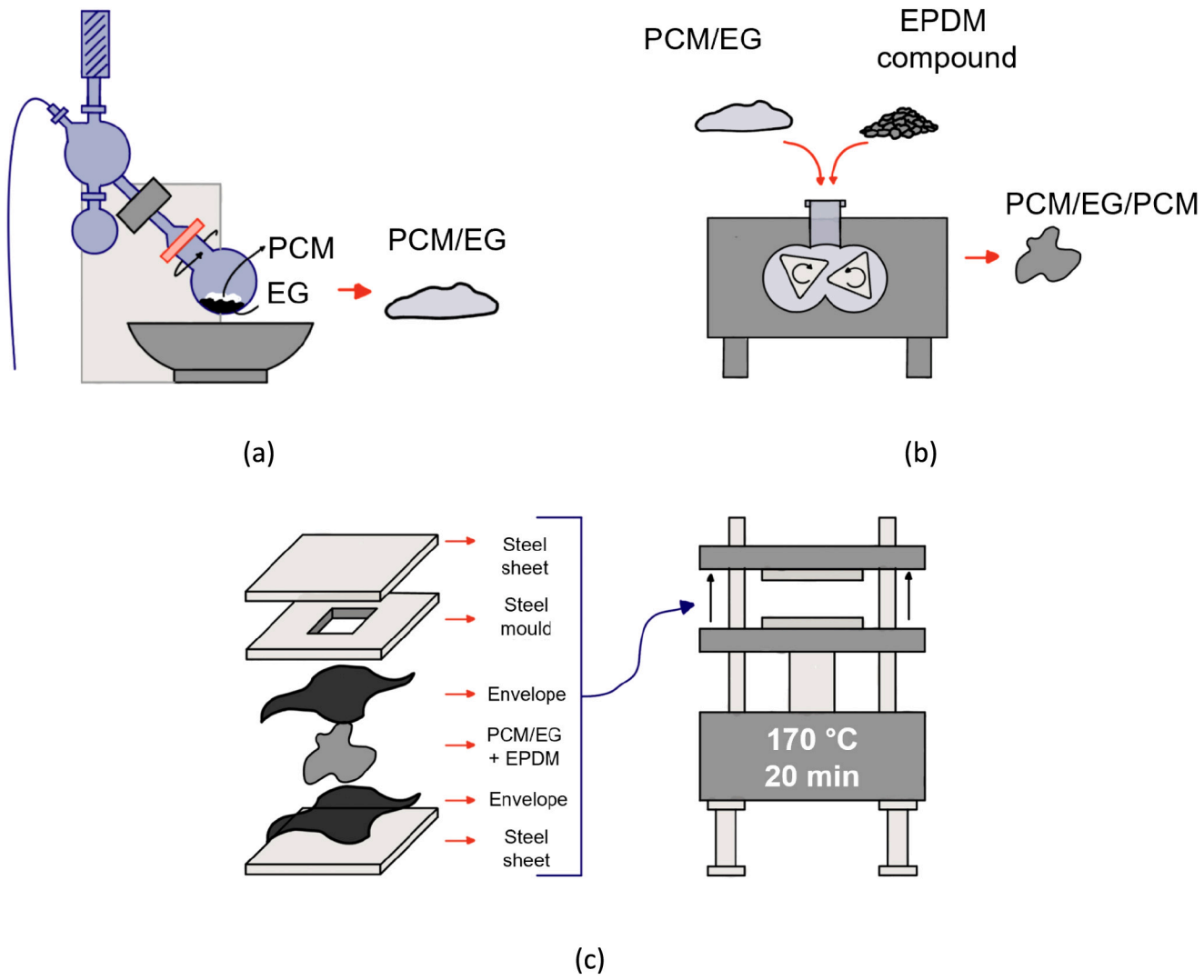

Fig. 1. Composite panel production scheme: a) PCM impregnation in EG by using Rotavapor; b) compounding; c) vulcanization and enveloped panel realization via hot compression moulding.

Table 1
Codes of PCM/EG samples.

Sample code	PCM content		EG content	
	(phr)	(wt%)	(phr)	(wt%)
RT28/8EG	100	92.6	8	7.4
RT28/10EG	100	90.9	10	9.1
RT28/12EG	100	89.3	12	10.7

the quantities listed in Table 2 using a Thermo Haake Rheomix 600 melt compounder (Thermo Fisher Scientific, USA) equipped with counter-rotating rotors (Fig. 1b). The process was conducted imposing a temperature of 50 °C into the mixing chamber and a rotor speed of 40 rpm. Initially, the EPDM rubber and carbon black were fed into the mixing chamber and processed for 5 min. Subsequently, the vulcanizing agents and additives were introduced, followed by an additional 5 min of mixing to ensure homogeneity of the elastomeric compound.

Table 2
Composition of the EPDM elastomeric compound.

Material	Quantity (phr)
Vistalon 2504	100
Sulfur	3
Zinc oxide	3
Stearic acid	1
Carbon black	20
Tetramethylthiuram disulfide (TMTD)	0.87
Zinc dibutyldithiocarbamate (ZDBC)	2.5

The preparation of the remaining compositions involved the gradual introduction of the PCM/EG powder into the mixing chamber at a rate of approximately 0.5 g/min. This controlled addition was critical to achieving a homogeneous dispersion within the EPDM matrix. Once the powder was fully incorporated, the blend underwent a final mixing stage for an additional 10 min to ensure a uniform distribution and complete amalgamation of the constituents.

Preliminary formulations were developed to optimize the EG content within the composite while maintaining a constant EPDM-to-PCM mass ratio of 100:263. This ratio was selected to replicate the elastomer-to-PCM proportions established in the study by Valentini et al. [28]. The masses of the EPDM compound and the PCM/EG were adjusted accordingly to satisfy the overall compositions detailed in Table 1. It is important to note that the samples listed in Table 3 incorporate two different carbonaceous fillers: carbon black, which serves as a reinforcing filler for the EPDM compound, and the expanded graphite, which acts as shape-stabilizer for the PCM while simultaneously

Table 3
Sample coding and compositions of preliminary formulations.

Sample code	EPDM compound (wt%)	PCM (wt%)	EG (wt%)
p-8EG	31.5	63.4	5.1
p-10EG	31.1	62.6	6.3
p-12EG	30.7	61.9	7.4

"p" stands for "preliminary formulation".

enhancing the thermal conductivity of the composite.

The final stage of composite panel fabrication involved vulcanization at a temperature of 170 °C under a load of 2 MPa for a duration of 20 min, using a Carver Hot press (Fig. 1c). The blend was placed into steel molds to produce panels with dimensions of 120 mm × 120 mm × 2 mm (preliminary compositions of Table 3) and 120 mm × 120 mm × 5 mm (refined compositions of Table 4). During this process, the samples were enclosed in nitrile butadiene rubber (NBR) envelopes that co-vulcanized with the internal EPDM matrix. This encapsulation strategy not only effectively prevented PCM leakage during the high-temperature curing process but also formed a durable, waterproof coating for the final composite panels [28].

Preliminary self-sustainment tests identified the 12:100 as the optimal EG-to-PCM ratio for ensuring structural integrity of the composite. Based on these results, three additional compositions were fabricated to investigate the effects of varying the PCM loadings; these formulations are detailed in Table 4. Fig. 2 illustrates the resulting samples from Table 4, showcasing the variations in PCM content and specimen dimensions.

2.3. Experimental methodologies

To verify the chemical structure of the neat PCM, Fourier-transform infrared (FTIR) spectroscopy was performed using a Spectrum One spectrometer (PerkinElmer) in Attenuated Total Reflection (ATR) mode (wavenumber range: 4000–640 cm^{-1}, four scans).

Following chemical characterization, the physical stability of the preliminary compositions was evaluated to determine the optimum EG-to-PCM ratio. Leakage test was carried out 12 °C above the melting temperature similarity to Das et al. [51], and three days was selected as time for reaching a plateau in PCM loss in EPDM-based compounds according to literature [42]. The test was conducted leaving specimens of dimensions 10 mm × 10 mm × 10 mm without envelopes into an oven at 40 °C for 72 h on a porous filter paper (Extra Rapida – Perfecte 2, provided by Gruppo Cordenons S.p.A., characterized by grammage of 90 g/m^2 and thickness 196 μm) to favour the PCM extraction, with mass measurements taken before and after the test.

A self-sustaining test was conducted according to an internal protocol to further assess structural integrity under selected conditions (40 °C for 72 h). Thin enveloped sheets (120 mm × 120 mm × 2 mm) were positioned at a 58° inclination and statically maintained to monitor potential deflection. This utilized a specialized support featuring two parallel rows of pins (2 mm diameter, 40 mm exposed length) spaced 25 mm apart in order to have a contact point at approximately two fifth of the panel length.

Once the optimal EG-to-PCM ratio of 12:100 was established through these stability tests, the influence of PCM content on the thermal and mechanical properties was investigated exclusively on the optimized formulations listed in Table 4. Thermogravimetric Analysis (TGA) was conducted to assess thermal stability using a Mettler TG50 thermobalance (Mettler-Toledo, Greifensee, Switzerland). Samples of approximately 10 mg of neat PCM and composite core material (collected after removing the NBR envelope) were heated from 30 °C to 700 °C at 10 °C/min under a nitrogen flux of 100 mL/min. From the thermograms some characteristic parameters were considered to compare the formulations: the temperature associated to the first (T_{p1}), second (T_{p2}), third (T_{p3}), and fourth (T_{p4}) degradation peaks, and residual mass at 700 °C (m_{700}).

Differential Scanning Calorimetry (DSC) was performed to determine the phase transition temperatures and enthalpies with a Mettler DSC30 calorimeter (Mettler-Toledo, Greifensee, Switzerland). Three thermal ramps at a constant rate of 1 °C/min were imposed, from 15 to 35 °C, composing a thermal cycle with two heating scans alternated by a cooling ramp, to simulate the working condition after resetting the thermal history of the material. The specimen mass was near 10 mg, inserted into 40 μL aluminum crucibles, and a nitrogen flux of 100 mL/min was imposed. The peak phase transition temperature (T_{m1}, T_c and T_{m2}) and enthalpies (ΔH_{m1}, ΔH_c, and ΔH_{m2}) were evaluated from the thermograms. To better appreciate the PCM effect into the composite material, the effective PCM content (PCM_{m2}^{eff}) and the efficiency of melting (η_{m2}) were evaluated in the second heating scan according to Eqs. (1) and (2).

$$PCM_{m2}^{eff} = \frac{\Delta H_{m2}}{\Delta H_{m2,PCM}} \cdot 100 \quad (1)$$

$$\eta_{m2} = \frac{\Delta H_{m2}}{\Delta H_{m2,PCM} \cdot W_{PCM}} \cdot 100 \quad (2)$$

where $\Delta H_{m2,PCM}$ is the specific enthalpy of the neat PCM in the second heating scan and W_{PCM} is the weight fraction of the PCM.

Thermophysical properties were determined at 10 °C, which is the temperature usually considered for conventional insulation materials [52]. Bulk density (ρ) was determined as ratio between mass, measured with a balance (sensitivity 0.1 mg), and the volume determined measuring with a calliper (resolution 0.1 mm). The specific heat capacity (c_p) was determined following the ASTM E1269–11 standard performing DSC ramps with a DSC5+ calorimeter (Mettler-Toledo, Greifensee, Switzerland) from 0 °C to 20 °C at 1 °C/min on three specimens of 10 mg for each sample. The heat flux at 10 °C was compared to that of a sapphire reference. Thermal diffusivity (α) was evaluated using a Laser Flash Analyzer (LFA) Neztsch LFA 446 (Selb, Germany). Three disks of diameter 12.7 mm and thickness 2.5 mm for each sample were tested imposing a laser signal of 250 V and pulse width of 0.6 ms. Thermal conductivity (λ) was determined as product of the thermophysical properties previously determined according to Eq. (3).

$$\lambda = \alpha \cdot \rho \cdot c_p \quad (3)$$

The results of all the thermophysical properties were reported as mean value ± standard deviation of the tested specimens.

To identify the optimal balance between enhanced heat transfer and storage capacity, the cooling capacity Figure of Merit (FoM) was determined according to Eq. (4) [53], allowing for a quantitative comparison between different systems.

$$FoM = \sqrt{\Delta H_m^* \cdot \lambda} \quad (4)$$

where ΔH_m^* is the volumetric latent heat of melting, calculated as the product of the mass-based enthalpy and bulk density.

Infrared (IR) thermography was conducted using a IRtech Fotric 348 A IR thermal imaging camera (Fotric, Santa Clara, CA, USA) on enveloped panels (120 mm × 120 mm × 5 mm) placed into a climatic chamber ACS Discovery DM340C (Angelantoni Industrie S.r.l., Massa Martana, Italy). A specimen for each formulation was compared to neat EPDM rubber, imposing a thermal cycle consisting of an isotherm at

Table 4
Sample coding and compositions of the optimized formulations.

Sample code	EPDM compound (wt%)	PCM (wt%)	EG (wt%)
EPDM-60RT28/12EG	32.8	60.0	7.2
EPDM-65RT28/12EG	27.2	65.0	7.8
EPDM-70RT28/12EG	21.6	70.0	8.4

Fig. 2. Representative image of EPDM-60RT28/12EG, EPDM-65RT28/12EG and EPDM-70RT28/12EG samples (left to right). Top: 120 mm × 120 mm × 5 mm panels. Bottom: 25 mm × 25 mm × 5 mm panels.

10 °C (60 min), followed by a ramp to 45 °C (60 min), isotherm at 45 °C (120 min), cooling back to 10 °C (60 min), and starting again with the isotherm at 10 °C (120 min). This testing protocol was designed to qualitatively and partially quantitatively verify the PCM effect in thermal regulation.

To complete the composite characterization and determine appropriate storage and transport conditions prior to construction, mechanical properties were evaluated via compression tests. These tests were conducted on disks (13 mm diameter, 3 mm thickness) at both room temperature (21 °C) and above the PCM phase transition temperature (40 °C). The tests were conducted using an Instron (Pianezza, Italy) 5969 testing machine equipped with a load cell of 50 kN and a climatic chamber, adopting a strain rate of 1 mm/min. The results were summarized extrapolating the following parameters from the compressive stress-strain curves: the compressive modulus (E) evaluated in the range of 0.05 and 0.1 mm/mm of strain, the deformation of the samples corresponding to a stress equal to 0.1 MPa ($\varepsilon_{0.1}$), and the stress corresponding to selected deformation of 0.10, 0.25, 0.50, and 0.75 mm/mm (coded $\sigma_{0.1}$, $\sigma_{0.25}$, $\sigma_{0.5}$, and $\sigma_{0.75}$, respectively). Three specimens for each sample were tested, and the results are reported as mean value ± standard deviation.

The analysis was further expanded by modelling the composite compressive modulus at room temperature, enabling the prediction of properties for compositions not covered in the experimental phase. In this model, the matrix was treated as a blend of PCM and EPDM; its modulus (E_m) was calculated using the Rule of Mixtures (Voigt model), as shown in Eq. (5).

$$E_m = E_{PCM} \cdot f_{PCM} + E_{EPDM} \cdot f_{EPDM} \tag{5}$$

where E_{PCM} and E_{EPDM} represent the experimental compressive moduli of the PCM and EPDM, respectively, measured under the same conditions as the composites. The terms f_{PCM} and f_{EPDM} denote the volume fractions of the PCM and EPDM, normalized specifically for the matrix phase.

The role of EG as a reinforcing filler was then evaluated using the Halpin-Tsai model (Eq. (6)).

$$E_c = E_m \frac{1 + \xi \eta f_{EG}}{1 - \eta f_{EG}} \tag{6}$$

where E_c is the compressive modulus of the composite, ξ is the reinforcing factor, η is the efficiency factor (Eq. (7)), and f_{EG} represent the volume fraction of EG.

$$\eta = \frac{\frac{E_{EG}}{E_m} - 1}{\frac{E_{EG}}{E_m} + \xi} \tag{7}$$

Combining and reversing Eqs. (6) and (7), it was possible to determine ξ for the composites (Eq. (8)) and construct the entire trend of E_c as a function of f_{EG}.

$$\xi = \frac{\frac{E_{EG}}{E_m}(E_c - E_m) - E_c f_{EG}\left(\frac{E_{EG}}{E_m} - 1\right)}{E_m f_{EG}\left(\frac{E_{EG}}{E_m} - 1\right) + E_m - E_c} \tag{8}$$

To appreciate the stiffness drop passing from solid to liquid state of the PCM, the compressive modulus of the composites was additionally normalized with respect to the neat EPDM ($E_{rel,21}$ and $E_{rel,40}$, respectively).

Regarding the technological properties of the final products, Shore A hardness test of neat EPDM and composite samples were conducted with and without NBR envelope. The tests were conducted at 21 °C using a Hildebrand durometer with an applied load of 488 g, following the ASTM D2240. The values were recorded after 5 s of contact between tip and sample. The results were reported as mean value ± standard deviation of 5 measurement.

Finally, some complementary parameters are evaluated to complete the overview of the technical properties of the final composite product: the surface density (*SD*), which represent the volumetric weight of a panel of thickness 5 mm, and the thermal management ability (*TMA*), which expresses the surface ability in absorbing heat of the panel of thickness 5 mm [54].

3. Results and discussion

3.1. Preliminary characterization and composition refinement

Following the identification of the PCM chemical structure (Fig. 3), this section evaluates the preliminary formulations to determine how the EG content affects the structural integrity of the composite panels. To ensure a reliable comparison, the PCM-to-elastomer ratio was maintained constant, consistent with previous studies where oMMT was employed as the shape-stabilizing agent [28].

The FTIR spectrum of RT28 exhibits the characteristic profile of an aliphatic hydrocarbon, showing a lack of polar functional groups, consistent with the profile of a paraffin. The intense peaks at 2914 and 2850 cm^{-1} are assigned to the asymmetric and symmetric C—H stretching vibrations, respectively. Furthermore, the peaks at 1471 and 716 cm^{-1} correspond to C—H bending and wagging vibrations [46,54].

Following this chemical identification, the investigation focused on phase transition leakage, which represents one of the primary challenges associated with the incorporation of PCMs into building components, strongly affecting their long-term thermal performance. As reviewed by

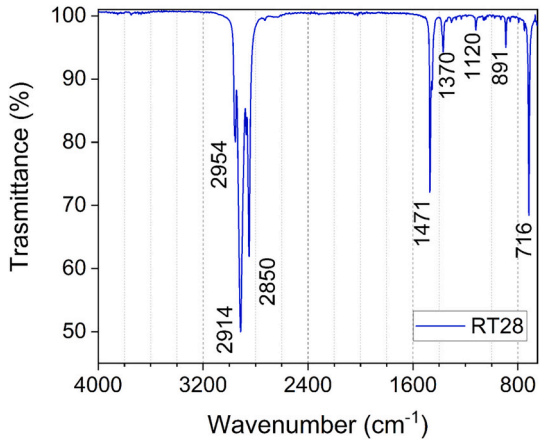

Fig. 3. FTIR spectrum of the selected PCM.

Wu et al. [55], direct immersion or simple impregnation techniques are increasingly avoided in construction due to high vulnerability to leakage and the lack of systematic mechanisms for long-term confinement. To overcome these limitations, research has oriented toward microencapsulation and form-stable composite matrices. More recently, macroencapsulation methods, such as embedding dedicated PCM pouches or bags into brick walls to physically isolate the organic phase, have been explored—a methodology extensively documented in a recent review by Lachheb et al. [56]. However, as highlighted by these state-of-the-art reviews, a significant discrepancy still exists between laboratory testing conditions and practical building applications, as leakage and containment stability under real operational thermal cycles have rarely been investigated via a systematic engineering approach. Since standardized protocols for leakage tests are currently unavailable in the literature, our preliminary tests were designed for identifying the minimum EG loading required to guarantee geometric and physical self-sustainment, in order to proceed for an extended processing. To this end, the mass of the unencapsulated samples was monitored before and after thermal exposure as a direct indicator of exudation. The experimental results are summarized in Table 5.

The analysis revealed no significant correlation between mass loss and EG content. Notably, the recorded total mass variation following accelerated thermal aging remained remarkably low, at approximately 0.5 wt% across all formulations, corresponding to about 0.7–1.0 wt% of the overall PCM. This minimal variation confirms the excellent thermal stability of the composite core, demonstrating that the shape-stabilization strategy effectively prevents PCM leakage under typical operating conditions. Crucially, *zero-leakage* conditions are achieved in the final product through the integration of the co-vulcanized NBR envelope, which forms a robust interfacial bond with the composite core, providing a structural barrier.

In parallel to mass stability, geometrical self-sustainment under high-temperature gravitational stress was evaluated on the "preliminary panels" 2 mm thick (p- EG), to identify the optimal EG content for ensuring structural stability. These tests assessed the ability of each composite to remain geometrically stable under prolonged temperature exposure at 40 °C for 72 h. Fig. 4a and b illustrate the deflection of the specimens before and after the test.

Table 5
Leaking test results at 40 °C after 72 h of preliminary formulation samples without envelope.

Sample code	Total mass loss (wt%)	Relative PCM loss (wt%)
p-8EG	- 0.45	- 0.71
p-10EG	- 0.64	- 1.02
p-12EG	- 0.57	- 0.92

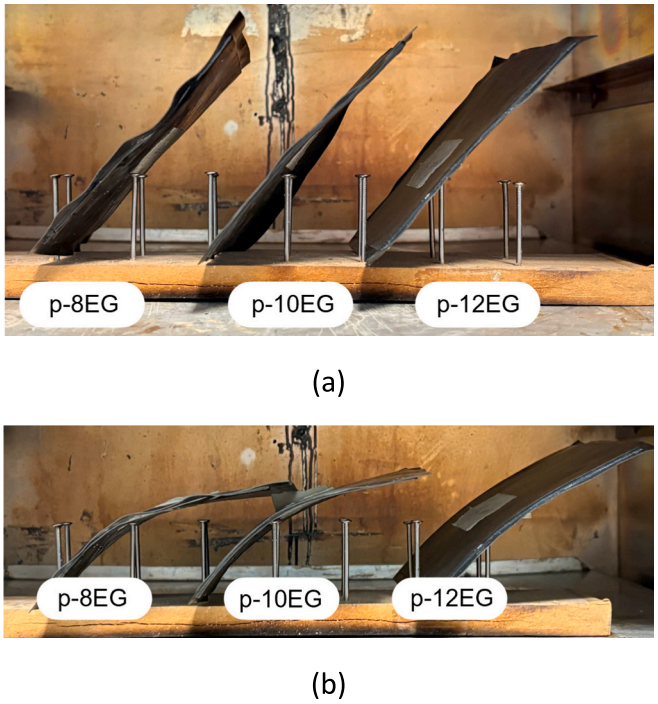

Fig. 4. Results of the form-stability test on composite panels (120 mm × 120 mm × 2 mm): (a) initial state; (b) after accelerated thermal aging at 40 °C for 72 h.

As shown in Fig. 4b, a clear distinction emerges based on the EG concentrations: the p-8EG and p-10EG samples display visible structural collapse and geometric distortion under their own weight once the PCM transitions to the liquid state. Conversely, the p-12EG sample exhibits superior shape retention and negligible deflection. This enhanced structural robustness is directly attributed to the higher EG loading (12 phr in RT28), which provides sufficient physical reinforcement to contain the PCM in its molten state.

Consequently, the 12 phr EG-to-PCM ratio was selected as the optimal baseline threshold for the refined formulations (Table 4). Further EG increments were avoided to prioritize the primary objective of maximizing the volumetric latent heat storage capacity. Interestingly, maintaining this precise ratio creates a minor excess of PCM relative to the absolute adsorption limits of the EG flakes, which proved beneficial during the compounding stage. Due to the high chemical affinity between the aliphatic paraffinic chains and the EPDM rubber, this non-adsorbed PCM fraction acts as a secondary processing aid. Instead of causing macro-segregation, it reduces melt viscosity during mixing, significantly improving filler dispersion, enhancing interfacial wetting, and ultimately ensuring a highly homogeneous composite structure suitable for reliable building-envelope applications.

3.2. *Thermophysical properties of refined compositions*

Following the optimization of the composite structural integrity, the thermal stability of the refined compositions was investigated. The thermal degradation behaviour of the neat PCM and composite panels is illustrated in Fig. 5, showing the residual mass (a) and its derivative (b) as function of temperature. The characteristic thermogravimetric results are summarized in Table 6.

As illustrated in the TGA curves of Fig. 5, the degradation onset occurs at approximately 100 °C, suggesting a potential partial degradation of the PCM during the hot-press vulcanization (170 °C). The degradation peak for the neat RT28, centred at about 250 °C, shifts toward lower temperatures in the composite formulations (reaching 213 °C for EPDM-

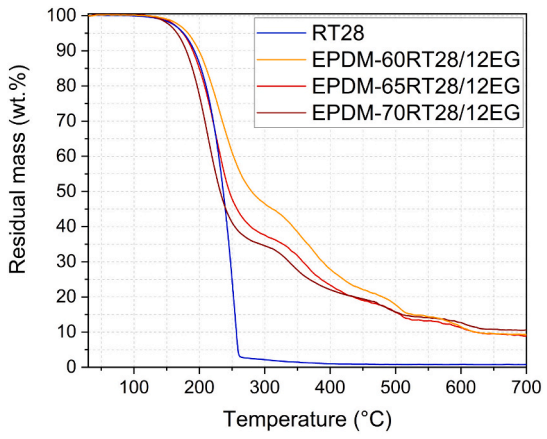

(a)

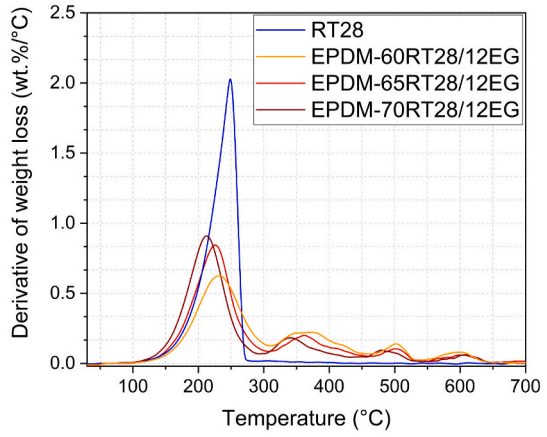

(b)

Fig. 5. TGA thermograms of refined formulations: (a) mass loss curves; (b) derivative of weight loss.

Table 6
Characteristic thermal degradation temperatures and residual mass of neat PCM and refined composite formulations obtained from TGA analysis.

SAMPLE	$T_{5\%}$ (°C)	T_{p1} (°C)	T_{p2} (°C)	T_{p3} (°C)	T_{p4} (°C)	m_{700} (wt%)
RT28	176	248	–	–	–	0.7
EPDM-60RT28/12EG	183	232	371	502	602	9.3
EPDM-65RT28/12EG	175	226	362	501	601	8.9
EPDM-70RT28/12EG	166	213	341	480	610	10.6

T_{p1} = temperature corresponding to the first degradation peak; T_{p2} = temperature corresponding to the second degradation peak; T_{p3} = temperature corresponding to the third degradation peak; T_{p4} = temperature corresponding to the fourth degradation peak; m_{700} = residual mass at 700 °C.

70RT28/12EG), although the onset temperature remains comparable. Complete PCM decomposition is observed by 300 °C across all samples. The residue at 700 °C corresponds to the combined fraction of EG and EPDM compound char [28]. Minor discrepancies in the expected proportionality of the EG content may be attributed to local material inhomogeneities, a common occurrence when testing milligram-scale composite specimens in TGA.

While TGA serves as a destructive technique necessary to quantify the actual phase fractions and assesses the degradation limits of the components, it does not capture the latent heat storage performance under working conditions. Therefore, DSC was performed to evaluate the phase change behaviour and thermal storage capacity of the stabilized systems. Unlike TGA, DSC analysis is representative of service conditions, as it monitors the energy response of the material within the operational temperature range where the PCM effectively functions as a thermal buffer. Fig. 6 shows the thermograms for the first heating (a), cooling (b), and second heating (c), with the corresponding thermal parameters summarized in Table 7.

The measured melting and crystallization enthalpies are generally consistent with the theoretical values, with minor deviations likely attributable to local material inhomogeneities. The incorporation of the PCM within the composite matrix induces a downward shift in the phase transition temperature, a phenomenon also observed in previous studies using oMMT as a stabilizing agent [28]. This thermal behaviour justifies the selection of RT28, as it ensures that the phase transition occurs within the thermal comfort zone for building applications.

Notably, while the melting enthalpies exceeding 100 J/g are seldom reported for PCM-based composites [57–60], the EPDM-70RT28/12EG formulation achieved a remarkable value of 167 J/g. To the best of the authors' knowledge, this represents a benchmark for EPDM-based PCM composites [61–65].

Building on these calorimetric results, the investigation was extended to evaluate the steady state thermophysical properties. Table 8 summarizes the properties of the optimized samples at 10 °C, comparing them with the neat EPDM compound to assess the impact of PCM and EG loading on the overall thermal performance.

No significant fluctuations in density were observed, despite the high PCM loading, which inherently reduces the density compared to the neat EPDM matrix. While these density values are approximately one order of magnitude higher than those of conventional insulation materials, this characteristic is not necessarily a drawback. Conventional insulation relies exclusively on low density and low thermal conductivity to minimize heat transfer—a strategy that is effective in winter but insufficient for summer thermal mitigation. Indeed, advanced insulation materials like aerogels, while efficient at retaining heat in winter due to their extremely low thermal conductivity, show negligible efficacy in summer due to their extremely low thermal admittance [43]. For effective summer mitigation, a material must possess sufficient thermal inertia to simultaneously store and conduct heat. In this regard, a slight reduction in specific heat capacity was observed, proportional to the increasing EG content; however, this effect is largely overcompensated by the structural and transport properties of the composite. Consequently, the relatively high density and the six-fold increase in thermal diffusivity provided by the EG network are essential; this enhancement is directly reflected in the significantly higher thermal conductivity values and allow the panels to promptly respond to thermal perturbations and channel the heat toward the PCM core. This ensures that the phase change transition is fully utilized to dampen daily temperature peaks. This performance level is substantially higher than that of PCMs directly incorporated into concrete or aggregates [66–68]. Since those low-energy-density cementitious systems have already proven effective at attenuating building temperature fluctuations [69], our optimized panels—leveraging a highly concentrated, record-high latent heat capacity—are consequently more effective at flattening indoor thermal peaks.

3.3. Thermal response of PCM-composite panels under dynamic cycling

The thermal response of the composite panels to external fluctuations was qualitatively evaluated via Infrared (IR) thermography during a controlled thermal cycle within a climatic chamber. Fig. 7 depicts the temperature-time profiles of the composite panels, while Fig. 8 displays representative IR images captured during the heating (a) and cooling (b) stages, providing a visual assessment of the temperature distribution across the panel surfaces.

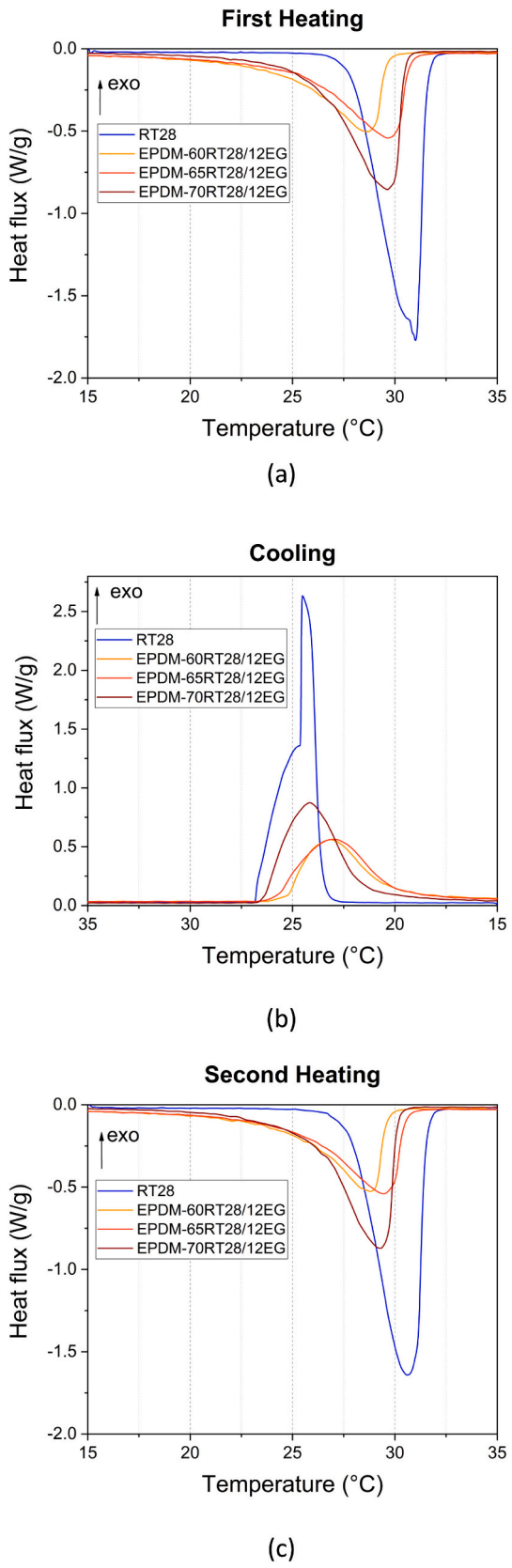

Fig. 6. DSC thermograms of refined compositions at 1 °C/min: (a) first heating; (b) cooling; (c) second heating.

Unlike the neat rubber compound, which exhibited a linear temperature response, the PCM-integrated samples maintained quasi-isothermal conditions during the phase transitions. This behaviour, illustrated in Fig. 7, confirms the thermal buffering capacity of the composites, as the latent heat absorption/release effectively stabilizes the panel temperature despite the external forcing. Specifically, at the minute 190 of test (first dashed line, Fig. 7), the temperature of the PCM-composite panels results 8.9 ± 0.2 °C lower than the reference neat EPDM; likewise, at minute 365 (second dashed line, Fig. 7), the heat-absorbing panels show a temperature higher of 9.1 ± 0.1 °C than neat EPDM.

Moreover, at an intermediate threshold of 30 °C, the PCM formulations demonstrated a thermal lag of approximately 25 min compared to the neat EPDM. While this delay might appear limited, it must be interpreted in the context of the high-power thermal forcing of the climatic chamber, which continuously compensates for the PCM's latent heat absorption. As such, these findings provide a qualitative validation of the buffering effect rather than a direct quantification of energy savings. Minor fluctuations during the 10 °C and 40 °C plateaus are simply attributed to the dynamic control logic of the chamber during transient stabilization. Despite these experimental constraints, the results clearly illustrate the material's ability to interfere with heat flux through phase transition.

To translate these laboratory results into practical building performance, future research will involve small-scale experimental units exposed to real-world summer conditions [43]. Monitoring internal air and surface temperatures under fluctuating solar radiation will allow for a precise quantification of the decrement factor and time lag, confirming the efficacy of these panels in improving indoor thermal comfort and reducing cooling energy demand. These qualitative findings represent a useful indicator for a quantitative evaluation in real scale applications.

3.4. *Compressive properties and elastic modulus modelling*

The compressive properties were determined to provide a comprehensive mechanical profile of these novel PCM composite panels. Specifically, the tests aimed to evaluate the structural response upon PCM liquefaction, providing critical data for the handling, storage, and transportation of the products prior to building integration. Understanding the mechanical stability at 40 °C is essential to ensure that the panels maintain their integrity under stacking loads when the latent heat storage component is in its molten state. The compressive stress-strain curves of the panels, evaluated at both room temperature (21 °C) and above the PCM phase transition (40 °C) are observable in Fig. 9, with the corresponding mechanical parameters summarized in Table 9 and 10.

In both cases, all the PCM composites at high strain exhibited lower compressive stress than EPDM (Fig. 9a and b). However, an inversion was observed at room temperature up to 0.35 mm/mm of compressive strain as shown in Fig. 9c, due to the presence of EG; as expected, the higher the temperature, the lower the compressive stress.

The temperature dependence of the mechanical response is clearly illustrated by the stress-strain curves in Fig. 9. As expected, the neat EPDM remains largely unaffected by these contained temperature fluctuations, exhibiting only minor variations in the initial stiffness, while at higher deformations the temperature clearly softens the compound. In contrast, the PCM-based panels undergo a significant softening upon reaching the phase transition temperature. This reduction in performance is directly attributed to the solid-to-liquid transition of the paraffin wax; as the PCM liquefies, its structural contribution is diminished, leading to a more compliant composite behaviour.

Despite the softening of the matrix above the melting point, all formulations maintained a compressive stress ($\sigma_{0.1}$) exceeding 0.1 MPa (equivalent to 10 ton/m^2) at 40 °C. While a 10% deformation is considered a relatively high threshold for structural assessment, these results guarantee that the panels can withstand significant static loads without structural failure. This ensures that the material maintains its

Table 7
Phase change properties of the neat PCM and composite formulations derived from DSC analysis conducted at 1 °C/min, including melting/crystallization temperatures and latent heat values.

Sample	T_{m1} (°C)	ΔH_{m1} (J/g)	T_c (°C)	ΔH_c (J/g)	T_{m2} (°C)	ΔH_{m2} (J/g)	PCM_{m2}^{eff} (%)	η_{m2} (%)
RT28	29.0	232.5	27.5	230.8	28.8	231.4	100	100
EPDM-60RT28/12EG	27.3	129.5	24.7	129.8	27.4	130.3	56.3	93.8
EPDM-65RT28/12EG	28.1	142.2	24.6	141.5	28.0	143.7	62.1	95.5
EPDM-70RT28/12EG	29.0	167.2	24.9	165.4	28.6	166.8	72.1	102.0

T_{m1} = melting peak temperature during the first heating scan; ΔH_{m1} = specific melting enthalpy during the first heating scan; T_c = crystallization peak temperature during cooling; ΔH_c = specific melting enthalpy during cooling; T_{m2} = melting peak temperature during the second heating scan; ΔH_{m2} = specific melting enthalpy during the second heating scan; PCM_{m2}^{eff} = effective PCM content from the second melting transition (Eq. (1)); η_{m2} = efficiency of melting in the second heating scan (Eq. (2)).

Table 8
Thermophysical properties at 10 °C.

Sample	ρ (g/cm^3)	c_p (J/g·K)	α (mm^2/s)	λ (W/m·K)
EPDM	1.00 ± 0.01	1.75 ± 0.02	0.14 ± 0.01	0.25 ± 0.01
EPDM-60RT28/12EG	0.92 ± 0.01	2.00 ± 0.04	0.89 ± 0.07	1.63 ± 0.13
EPDM-65RT28/12EG	0.91 ± 0.01	1.98 ± 0.03	0.93 ± 0.11	1.68 ± 0.22
EPDM-70RT28/12EG	0.93 ± 0.01	1.95 ± 0.06	0.91 ± 0.02	1.65 ± 0.14

ρ = bulk density; c_p = specific heat capacity; α = thermal diffusivity; λ = thermal conductivity.

integrity during stocking and transport under summer conditions, preventing permanent damage when the PCM is liquefied and the matrix is at its most compliant state.

Details on initial step (relative stiffness) Fig. 9c and d reveal a distinct mechanical trend compared to previous systems with organo-modified montmorillonite (oMMT), likely due to the superior structural reinforcement and stabilizing effect provided by the carbon-based network [28]. Notably, EPDM-70RT28/12EG formulation exhibits mechanical properties comparable to those of EPDM-60RT28/12EG, highlighting the critical role of EG in sustain the matrix stiffness despite the high PCM loading.

In particular, the stiffness exhibits a linear dependence on the EG content at temperatures both above and below the PCM phase transition. However, at higher deformations, the EPDM-65RT28/12EG formulation shows lower mechanical performance than expected relative to the formulations with higher PCM loading. This deviation suggests potential localized inhomogeneities or minor processing inconsistencies during the compounding of this specific sample. Interestingly, this mechanical discrepancy tends to diminish when transitioning from 21 °C to 40 °C. This convergence at higher temperatures indicates that once the PCM liquefies, the global response becomes increasingly dominated by the percolative EG network, which effectively masks the initial experimental variations observed at room temperature.

Regarding the analytical modelling of the compressive modulus, E_{PCM} and E_{EG} at 21 °C were determined as 1.8 ± 0.5 MPa and 250 ± 30 MPa, respectively. Starting from these values, the equivalent compressive moduli of the composite matrices were estimated using the Rule of Mixtures (RoM). Subsequently, the Halpin–Tsai micromechanical model was applied to predict the EG-dependent modulus trend for the final composites. The resulting theoretical predictions are compared with

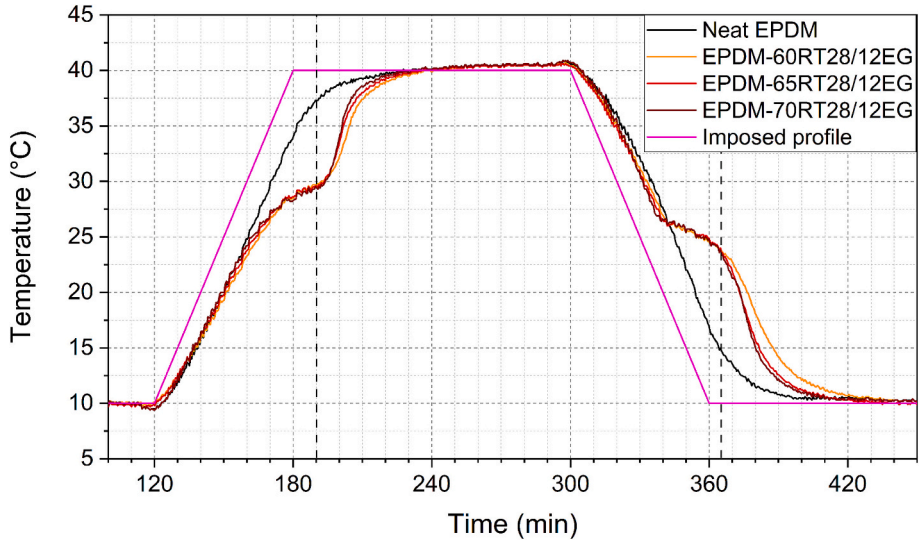

Fig. 7. Mean temperature profile of the composite sample recorded with the IR thermal camera during the cycle into the climatic chamber. The evidenced dotted lines correspond to the time at which the frames of Fig. 8 were captured.

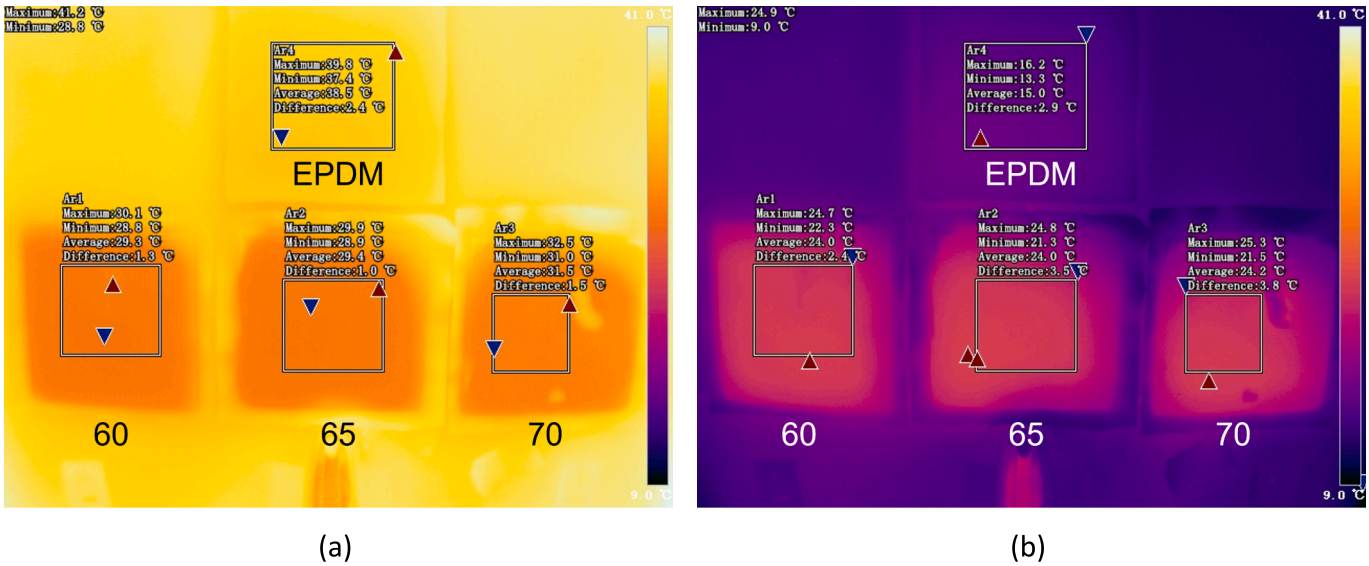

Fig. 8. Representative IR thermography images of the thermal cycle during of the composite panels with NBR envelope: (a) cooling (190 min); (b) during heating (365 min). In the images a simplified coding was adopted for neat EPDM compound (EPDM), EPDM-60RT28/EG12 (60), EPDM-65RT28/EG12 (65), and EPDM-70RT28/EG12 (70).

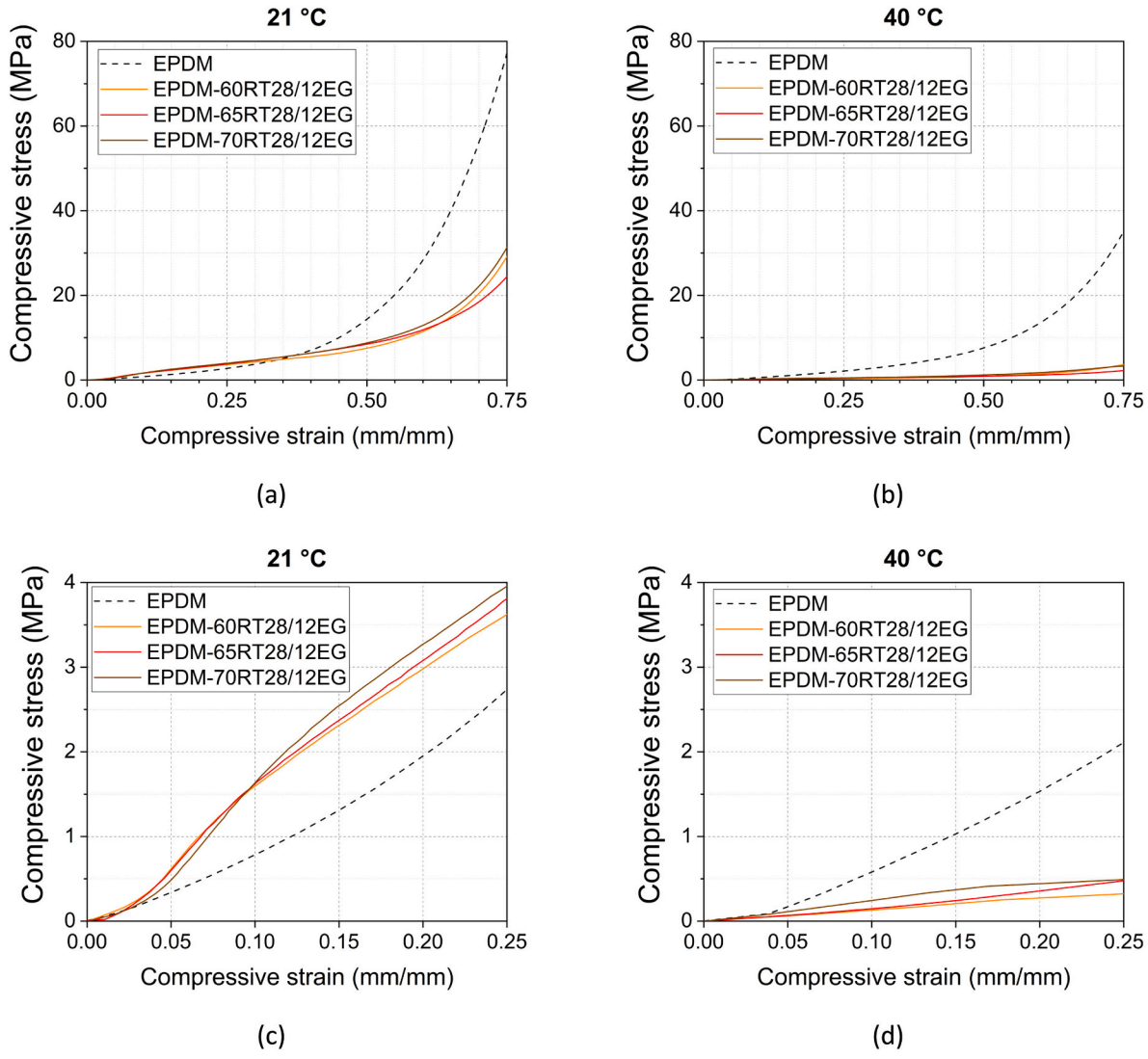

Fig. 9. Representative stress-strain compressive curves of neat EPDM and composite materials at 21 °C (a,c) and 40 °C (b,d) at different scales. Full range on the top (a, b); zoom of 0–0.25 strain on the bottom (c, d).

Table 9
Mechanical properties evaluated at 21 °C.

Sample	E [MPa]	$\varepsilon_{0.1}$ [%]	$\sigma_{0.1}$ [MPa]	$\sigma_{0.25}$ [MPa]	$\sigma_{0.50}$ [MPa]	$\sigma_{0.75}$ [MPa]
EPDM	10.6 ± 1.0	0.115 ± 0.011	0.87 ± 0.12	2.9 ± 0.2	15.0 ± 0.5	76.0 ± 8.0
EPDM-60RT28/EG	16.7 ± 0.7	0.068 ± 0.004	1.60 ± 0.09	3.7 ± 0.1	8.6 ± 0.9	31.5 ± 2.4
EPDM-65RT28/EG	17.3 ± 3.8	0.083 ± 0.014	1.31 ± 0.27	3.5 ± 0.3	7.1 ± 0.1	24.6 ± 2.0
EPDM-70RT28/EG	19.3 ± 1.8	0.068 ± 0.003	1.66 ± 0.12	3.8 ± 0.2	8.6 ± 0.4	29.9 ± 2.0

E = compressive elastic modulus; $\varepsilon_{0.1}$ = deformation at 0.1 MPa; $\sigma_{0.1}$ = stress at 0.1 mm/mm; $\sigma_{0.25}$ = stress at 0.25 mm/mm; $\sigma_{0.5}$ = stress at 0.5 mm/mm; $\sigma_{0.75}$ = stress at 0.75 mm/mm.

Table 10
Mechanical properties evaluated at 40 °C.

Sample	E [MPa]	$\varepsilon_{0.1}$ [%]	$\sigma_{0.1}$ [MPa]	$\sigma_{0.25}$ [MPa]	$\sigma_{0.50}$ [MPa]	$\sigma_{0.75}$ [MPa]
EPDM	8.3 ± 0.5	0.145 ± 0.005	0.58 ± 0.03	2.0 ± 0.1	7.3 ± 0.5	35.0 ± 2.0
EPDM-60RT28/EG	1.6 ± 0.4	0.542 ± 0.037	0.14 ± 0.01	0.3 ± 0.1	0.8 ± 0.1	3.4 ± 0.8
EPDM-65RT28/EG	1.8 ± 0.3	0.554 ± 0.023	0.17 ± 0.01	0.4 ± 0.1	0.9 ± 0.1	2.0 ± 0.3
EPDM-70RT28/EG	2.4 ± 0.3	0.463 ± 0.009	0.22 ± 0.01	0.5 ± 0.1	1.1 ± 0.1	3.2 ± 0.1

E = compressive elastic modulus; $\varepsilon_{0.1}$ = deformation at 0.1 MPa; $\sigma_{0.1}$ = stress at 0.1 mm/mm; $\sigma_{0.25}$ = stress at 0.25 mm/mm; $\sigma_{0.5}$ = stress at 0.5 mm/mm; $\sigma_{0.75}$ = stress at 0.75 mm/mm.

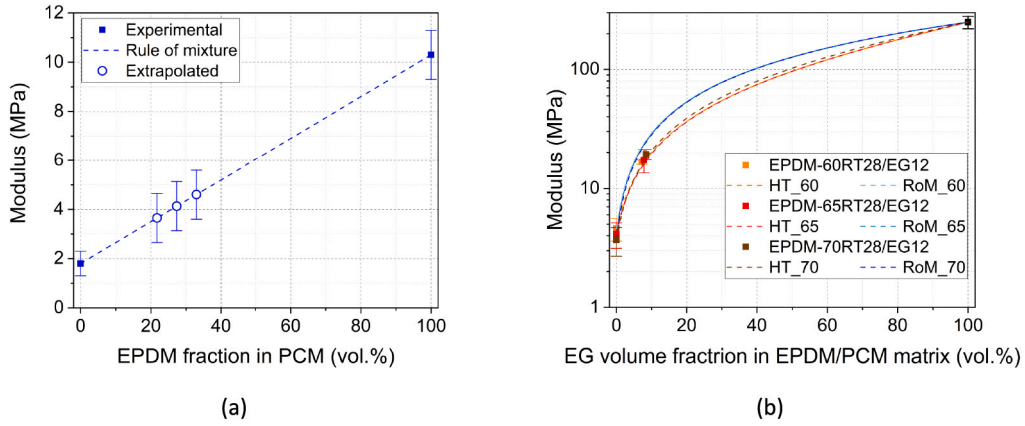

Fig. 10. Analytical modelling of the compressive moduli: a) equivalent modulus of the EPDM/PCM matrix estimated via the Rule of Mixtures (RoM); b) comparison between experimental results and theoretical predictions for the final composites using the Halpin–Tsai (HT) and RoM models.

experimental data in Fig. 10 and summarized in Table 11.

The analytical modelling further validates the good performance of the composites, with the reinforcing factor (ξ) reaching their peak values in the EPDM-70RT28/14EG formulation (3.6 vol%). This significant upward trend indicates a remarkably high reinforcing contribution from the EG at this concentration, confirming a powerful synergistic effect between the EPDM compound and the EG. These results demonstrate that an optimized filler network not only stabilizes the PCM but also substantially upgrades the mechanical robustness of the panel, surpassing the standard theoretical predictions. This synergy suggests that the 3.6 vol% threshold represents an ideal configuration for achieving a superior, high-integrity thermal management material.

Finally, it is noteworthy that this study provides a comprehensive mechanical assessment of EPDM/PCM/EG composites, addressing a significant gap in current literature. While comparative studies on organic PCMs within similar matrices often overlook mechanical characterization, existing research—primarily focused on systems incorporating polyethylene as an additional phase—reports tensile strengths in the range of 10 MPa [61,64]. By establishing these benchmarks for compressive strength and elastic modulus, this work not only demonstrates the feasibility of high-loading PCM-based composites, but also provides the necessary engineering data to transition these materials from laboratory prototypes to reliable building components.

3.5. Comparative analysis and benchmarking

A review of current literature reveals that composite panels frequently exhibit latent heat capacities below 100 J/g [70–72]. By benchmarking the EPDM-70RT28/12EG formulation against various state-of-the-art organic PCMs integrated into EG and EPDM matrices (Table 12), several key advancements emerge.

First, while many existing studies utilize PCM transition temperatures that are unsuitable for human thermal comfort, the current work specifically targets the building regulation zone using RT28. Notably, the developed composite achieves a benchmark melting enthalpy of 167 J/g, the highest among the compared materials in the literature. Furthermore, while some studies may report higher absolute thermal conductivities through extreme filler loading, this work achieves a superior functional balance. By increasing the conductivity by one order of magnitude relative to the neat PCM, the panels ensure a rapid thermal response without compromising the record-high energy storage density required for high-performance building envelopes.

The Figure of Merit (FoM) values substantiate the significant progress achieved in this study regarding building mitigation applications. While some FoM values reported in broader literature may appear comparable or even higher, they typically refer to composites utilizing high-temperature PCMs intended for industrial heat recovery rather than residential comfort. It is noteworthy that the current body of

Table 11
Results of the compressive moduli.

Sample	E_m (MPa)	ξ (/)	η (/)
EPDM-60RT28/EG14	4.6 ± 1.0	79	0.40
EPDM-65RT28/EG14	4.1 ± 1.0	89	0.39
EPDM-70RT28/EG14	3.7 ± 1.0	134	0.33

E_m = Compressive modulus of the matrix (RoM); ξ = reinforcing factor (HT); η = efficiency factor (HT).

Table 12
Thermophysical properties of representative studies in which organic PCM was integrated in the EG and EPDM matrix compared to composite panels of present study and preceding EPDM/oMMT stabilization.

Stabilizing constituents	Application	T_m (°C)	ΔH_m (J/g)	λ (W/m·K)	*FoM* (W/(m^2·K$^{0.5}$·s$^{0.5}$))	Reference
EPDM/PE	Photo-thermal conversion	70	139	2.1	$1.7 \cdot 10^4$	[61]
EPDM/PE/EG/CNT	Photo-thermal conversion	64	130	3.1	$2.0 \cdot 10^4$	[64]
EPDM/EG	Thermoelectric generation	62	133	2.1	$1.7 \cdot 10^4$	[63]
EPDM/EG	Generic thermal management	60	132	0.9	$1.1 \cdot 10^4$	[62]
EPDM/GMP	Light-thermal conversion	58	106	1.5	$1.2 \cdot 10^4$	[49]
EPDM/EG	Generic thermal management	48	113	2.5	$1.7 \cdot 10^4$	[65]
EPDM/oMMT	Building mitigation	25	126	0.7	$0.9 \cdot 10^4$	[28]
EPDM-60RT28/12EG	Building mitigation	27	130	1.6	$1.4 \cdot 10^4$	This paper
EPDM-65RT28/12EG	Building mitigation	28	144	1.7	$1.6 \cdot 10^4$	This paper
EPDM-70RT28/12EG	Building mitigation	29	167	1.7	$1.7 \cdot 10^4$	This paper

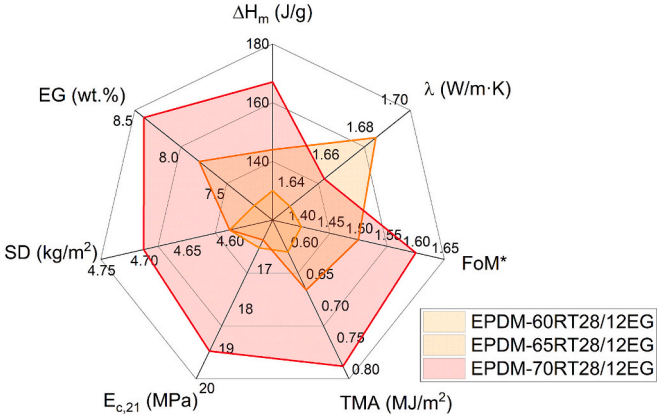

Fig. 11. Summary spider plot of the representative properties of the realized composites.

literature focusing specifically on the EPDM/PCM/EG system for building-range temperatures is remarkably scarce, with only a single previous study exploring this configuration.

By addressing this research gap, the present work establishes a new performance benchmark for low-temperature thermal management. In particular, comparing the thermophysical properties of the pioneering work for PCM melting in the 25–30 °C range [28], several advancements are evident. The strategic substitution of oMMT with EG as a shape stabilizer permits a simultaneous enhancement of both the PCM loading—and consequently the composite melting enthalpy—and the thermal conductivity. This dual improvement yields a markedly higher FoM, demonstrating a superior synergy between record-high latent heat and enhanced thermal transport, specifically optimized for the narrow temperature thresholds required in sustainable architecture.

To synthesize the performance profile of the heat-absorbing composite panels developed in this study, Fig. 11 provides a graphical comparison of their primary functional features. Furthermore, Table 13 presents a comprehensive technical datasheet of the optimized formulations, highlighting the significant property enhancements achieved relative to the neat EPDM control panels.

4. Conclusions

The fabrication of novel EPDM-based composite panels for building thermal management in temperature range 22–31 °C was successfully achieved by incorporating a paraffin with melting enthalpy peak of 28 °C in expanded graphite (EG). The dual role of EG as both a conductive filler and a shape-stabilizing agent enabled an exceptionally high PCM loading of 70 wt%, yielding a benchmark melting enthalpy of 167 J/g. By optimizing an EG-to-PCM ratio at 12:100, the composite achieved structural stability and a robust conductive network, which increases thermal conductivity to 1.7 W/m·K.

This combination of high latent heat and enhanced transport properties represents a significant advancement over traditional building materials. Crucially, while conventional insulation relies on low density

Table 13
Summary of the technological properties of the final products (rubber panels filled with Phase Change Material and expanded graphite).

Formulation	PCM content (vol%)	EG content (vol%)	Shore A* (/)	Shore A** (/)	$E_{rel,21}$ (/)	$E_{rel,40}$ (/)	*SD* (kg/m^2)	*TMA* (MJ/m^2)
EPDM	0	0	61 ± 1	–	1	1	5.00	0
EPDM-60RT28/EG12	64.9	3.1	73 ± 3	81 ± 3	1.58	0.19	4.60	0.60
EPDM-65RT28/EG12	70.2	3.4	76 ± 6	84 ± 2	1.56	0.22	4.55	0.66
EPDM-70RT28/EG12	75.4	3.6	74 ± 4	82 ± 3	1.82	0.29	4.65	0.78

$E_{rel,21}$ = normalized compressive modulus with respect to neat EPDM at 21 °C; $E_{rel,40}$ = normalized compressive modulus with respect to neat EPDM at 40 °C; *SD* = surface density for panels of thickness 5 mm; *TMA* = Thermal management ability of the panel (thickness 5 mm).

* Without NBR envelope.

** With NBR envelope.

to minimize winter heat loss, it remains largely ineffective against summer thermal loads due to a lack of thermal inertia. In contrast, the developed EPDM composites leverage their high thermal admittance to actively dampen daily temperature peaks. Qualitative tests in a climatic chamber clearly evidenced a thermal management action that delayed the temperature variation by 25 min at approximately 27 °C, during both heating and cooling.

A key contribution of this work lies in addressing a critical gap in recent literature. While contemporary state-of-the-art studies exploring carbonaceous-elastomeric blends are strictly tailored for high-temperature applications (such as battery and photovoltaic thermal management operating between 40 °C and 75 °C), these novel panels are uniquely optimized for the ambient indoor comfort range (22–31 °C). Strategic substitution of traditional clay-based supports (oMMT) with a percolative EG network successfully resolved the dual challenge of low thermal transport and limited PCM absorption capacities inherent to previous building-envelope configurations, as confirmed by the superior performance in the Figure of Merit (FoM) analysis.

Among the evaluated formulations, EPDM-70RT28/EG12 emerged as the optimal composition, exhibiting a superior balance between latent heat storage capacity, enhanced thermal conductivity, and structural integrity, maintaining a compressive strength exceeding 0.1 MPa even when the PCM is fully molten. While further EG increments could theoretically enhance thermal and mechanical performances, excessive loading was found to compromise the manufacturing process, resulting in poor mixing and non-uniform phase distribution.

Despite the great progress both in preparation methodologies and in the determination of the thermophysical properties of PCM samples, the advanced multifunctional applications of PCMs, in particular in building sector, require further exploration. Future research will focus on evaluating the thermal mitigation efficiency of these composites within small-scale building units under real-world summer conditions, providing a dynamic alternative to static insulation strategies.

CRediT authorship contribution statement

Sereno Sacchet: Writing – original draft, Validation, Methodology, Investigation, Formal analysis, Data curation, Conceptualization. **Alessandro Pizzato:** Writing – original draft, Investigation, Formal analysis. **Francesco Valentini:** Writing – original draft, Validation, Methodology, Formal analysis, Conceptualization. **Maurizio Grigiante:** Writing – review & editing, Supervision. **Riccardo Po:** Writing – review & editing, Supervision, Funding acquisition. **Luca Fambri:** Writing – review & editing, Supervision, Funding acquisition.

Declaration of competing interest

The authors declare that they have no known competing financial interests or personal relationships that could have appeared to influence the work reported in this paper.

Data availability

Data will be made available on request.

References

[1] U. Berardi, A cross-country comparison of the building energy consumptions and their trends, Resour. Conserv. Recycl. 123 (2017) 230–241, https://doi.org/10.1016/j.resconrec.2016.03.014.

[2] eurostat, Energy consumption in households. https://ec.europa.eu/eurostat/statistics-explained/index.php?title=Energy_consumption_in_households, 2024. (Accessed 5 December 2025).

[3] B.P.I.E. (BPIE), 97% of Buildings in the EU need to be updated. https://bpie.eu/wp-content/uploads/2017/12/State-of-the-building-stock-briefing_Dic6.pdf, 2017. (Accessed 9 December 2025).

[4] L. Mazzarella, Energy retrofit of historic and existing buildings. The legislative and regulatory point of view, Energy Build. 95 (2015) 23–31, https://doi.org/10.1016/j.enbuild.2014.10.073.

[5] F. Valentini, G. Maracchini, R. di Filippo, A. Dorigato, O. Bursi, A prospective life cycle assessment of insulation and window systems under evolving electricity and recycling scenarios for building energy retrofit in Italy, Energy Build. 347 (2025) 116245, https://doi.org/10.1016/j.enbuild.2025.116245.

[6] I.E.A. (IEA), RePowerEU Plan: Joint European action on renewable energy and energy efficiency. https://www.iea.org/policies/15691-repowereu-plan-joint-european-action-on-renewable-energy-and-energy-efficiency, 2023. (Accessed 9 December 2025).

[7] E. Commission, REPowerEU. https://reform-support.ec.europa.eu/document/download/c58a5fce-0504-4852-89bb-f51a16131c5a_en?filename=REPowerEU%20TSI_Final%20synthesis%20report_0.pdf, 2023. (Accessed 9 December 2025).

[8] M. Haller, S. Ludig, N. Bauer, Decarbonization scenarios for the EU and MENA power system: considering spatial distribution and short term dynamics of renewable generation, Energy Policy 47 (2012) 282–290, https://doi.org/10.1016/j.enpol.2012.04.069.

[9] A. Adesina, Use of phase change materials in concrete: current challenges, Renew. Energy Environ. Sustain. 4 (2019), https://doi.org/10.1051/rees/2019006.

[10] A. D'Alessandro, A.L. Pisello, C. Fabiani, F. Ubertini, L.F. Cabeza, F. Cotana, Multifunctional smart concretes with novel phase change materials: mechanical and thermo-energy investigation, Appl. Energy 212 (2018) 1448–1461, https://doi.org/10.1016/j.apenergy.2018.01.014.

[11] P. Sukontasukkul, T. Sutthiphasilp, W. Chalodhorn, P. Chindaprasirt, Improving thermal properties of exterior plastering mortars with phase change materials with different melting temperatures: paraffin and polyethylene glycol, Adv. Build. Energy Res. 13 (2) (2019) 220–240, https://doi.org/10.1080/17512549.2018.1488614.

[12] M. Kheradmand, M. Azenha, J.L.B. de Aguiar, J. Castro-Gomes, Experimental and numerical studies of hybrid PCM embedded in plastering mortar for enhanced thermal behaviour of buildings, Energy 94 (2016) 250–261, https://doi.org/10.1016/j.energy.2015.10.131.

[13] M.J. Abden, Z. Tao, Z. Pan, L. George, R. Wuhrer, Inclusion of methyl stearate/diatomite composite in gypsum board ceiling for building energy conservation, Appl. Energy 259 (2020) 114113, https://doi.org/10.1016/j.apenergy.2019.114113.

[14] X. Wang, H. Yu, L. Li, M. Zhao, Experimental assessment on the use of phase change materials (PCMs)-bricks in the exterior wall of a full-scale room, Energ. Convers. Manag. 120 (2016) 81–89, https://doi.org/10.1016/j.enconman.2016.04.065.

[15] A. Sharma, V.V. Tyagi, C.R. Chen, D. Buddhi, Review on thermal energy storage with phase change materials and applications, Renew. Sustain. Energy Rev. 13 (2) (2009) 318–345, https://doi.org/10.1016/j.rser.2007.10.005.

[16] R.A. Lawag, H.M. Ali, Phase change materials for thermal management and energy storage: a review, J. Energy Storage 55 (2022) 105602, https://doi.org/10.1016/j.est.2022.105602.

[17] V. Goel, A. Dwivedi, R. Kumar, R. Kumar, A.K. Pandey, K. Chopra, V.V. Tyagi, PCM-assisted energy storage systems for solar-thermal applications: review of the associated problems and their mitigation strategies, J. Energy Storage 69 (2023) 107912, https://doi.org/10.1016/j.est.2023.107912.

[18] A. Mahdavi, M. Farhadi, M. Gorji-Bandpy, A. Mahmoudi, A review of passive cooling of photovoltaic devices, Clean. Eng. Technol. 11 (2022) 100579, https://doi.org/10.1016/j.clet.2022.100579.

[19] P.K.S. Rathore, S.K. Shukla, Potential of macroencapsulated PCM for thermal energy storage in buildings: a comprehensive review, Construct. Build. Mater. 225 (2019) 723–744, https://doi.org/10.1016/j.conbuildmat.2019.07.221.

[20] M. Song, F. Niu, N. Mao, Y. Hu, S. Deng, Review on building energy performance improvement using phase change materials, Energ. Buildings 158 (2018) 776–793, https://doi.org/10.1016/j.enbuild.2017.10.066.

[21] A. Wazeer, A. Das, C. Abeykoon, A. Sinha, A. Karmakar, Phase change materials for battery thermal management of electric and hybrid vehicles: a review, Energy Nexus 7 (2022) 100131, https://doi.org/10.1016/j.nexus.2022.100131.

[22] V.J. Reddy, M.F. Ghazali, S. Kumarasamy, Advancements in phase change materials for energy-efficient building construction: a comprehensive review, J. Energy Storage 81 (2024) 110494, https://doi.org/10.1016/j.est.2024.110494.

[23] B. He, V. Martin, F. Setterwall, Phase transition temperature ranges and storage density of paraffin wax phase change materials, Energy 29 (11) (2004) 1785–1804, https://doi.org/10.1016/j.energy.2004.03.002.

[24] H. Bo, E.M. Gustafsson, F. Setterwall, Tetradecane and hexadecane binary mixtures as phase change materials (PCMs) for cool storage in district cooling systems, Energy 24 (12) (1999) 1015–1028, https://doi.org/10.1016/S0360-5442(99)00055-9.

[25] S. Peng, A. Fuchs, R.A. Wirtz, Polymeric phase change composites for thermal energy storage, J. Appl. Polym. Sci. 93 (3) (2004) 1240–1251, https://doi.org/10.1002/app.20578.

[26] A.M. Borreguero, M. Carmona, M.L. Sanchez, J.L. Valverde, J.F. Rodriguez, Improvement of the thermal behaviour of gypsum blocks by the incorporation of microcapsules containing PCMS obtained by suspension polymerization with an optimal core/coating mass ratio, Appl. Therm. Eng. 30 (10) (2010) 1164–1169, https://doi.org/10.1016/j.applthermaleng.2010.01.032.

[27] W. Mhike, W.W. Focke, J.P. Mofokeng, A.S. Luyt, Thermally conductive phase-change materials for energy storage based on low-density polyethylene, soft Fischer–Tropsch wax and graphite, Thermochim. Acta 527 (2012) 75–82, https://doi.org/10.1016/j.tca.2011.10.008.

[28] F. Valentini, A. Dorigato, L. Fambri, M. Bersani, M. Grigiante, A. Pegoretti, Production and characterization of novel EPDM/NBR panels with paraffin for potential thermal energy storage applications, Therm. Sci. Eng. Progress 32 (2022) 101309, https://doi.org/10.1016/j.tsep.2022.101309.
[29] G. Song, S. Ma, G. Tang, Z. Yin, X. Wang, Preparation and characterization of flame retardant form-stable phase change materials composed by EPDM, paraffin and nano magnesium hydroxide, Energy 35 (5) (2010) 2179–2183, https://doi.org/10.1016/j.energy.2010.02.002.
[30] C. Alkan, K. Kaya, A. Sarı, Preparation, thermal properties and thermal reliability of form-stable paraffin/polypropylene composite for thermal energy storage, J. Polym. Environ. 17 (4) (2009) 254–258, https://doi.org/10.1007/s10924-009-0146-7.
[31] W.-l. Cheng, R.-m. Zhang, K. Xie, N. Liu, J. Wang, Heat conduction enhanced shape-stabilized paraffin/HDPE composite PCMs by graphite addition: preparation and thermal properties, Sol. Energy Mater. Sol. Cells 94 (10) (2010) 1636–1642, https://doi.org/10.1016/j.solmat.2010.05.020.
[32] H. Inaba, P. Tu, Evaluation of thermophysical characteristics on shape-stabilized paraffin as a solid-liquid phase change material, Heat Mass Transf. 32 (4) (1997) 307–312, https://doi.org/10.1007/s002310050126.
[33] K. Kaygusuz, A. Sari, High density polyethylene/paraffin composites as form-stable phase change material for thermal energy storage, Energy Sour. Part A Recover. Utilization Environ. Eff. 29 (3) (2007) 261–270, https://doi.org/10.1080/009083190957568.
[34] K. Kaygusuz, C. Alkan, A. Sari, O. Uzun, Encapsulated fatty acids in an acrylic resin as shape-stabilized phase change materials for latent heat thermal energy storage, Energy Sour. Part A Recover. Utilization Environ. Eff. 30 (11) (2008) 1050–1059, https://doi.org/10.1080/15567030701258212.
[35] J. Kośny, K. Biswas, W. Miller, S. Kriner, Field thermal performance of naturally ventilated solar roof with PCM heat sink, Sol. Energy 86 (9) (2012) 2504–2514, https://doi.org/10.1016/j.solener.2012.05.020.
[36] K.A.R. Ismail, C.T. Salinas, J.R. Henriquez, Comparison between PCM filled glass windows and absorbing gas filled windows, Energy Build. 40 (5) (2008) 710–719, https://doi.org/10.1016/j.enbuild.2007.05.005.
[37] R. Baetens, B.P. Jelle, A. Gustavsen, Phase change materials for building applications: a state-of-the-art review, Energy Build. 42 (9) (2010) 1361–1368, https://doi.org/10.1016/j.enbuild.2010.03.026.
[38] L. Navarro, A. de Gracia, D. Niall, A. Castell, M. Browne, S.J. McCormack, P. Griffiths, L.F. Cabeza, Thermal energy storage in building integrated thermal systems: a review. Part 2. Integration as passive system, Renew. Energy 85 (2016) 1334–1356, https://doi.org/10.1016/j.renene.2015.06.064.
[39] L.F. Cabeza, A. Castell, C. Barreneche, A. de Gracia, A.I. Fernández, Materials used as PCM in thermal energy storage in buildings: a review, Renew. Sustain. Energy Rev. 15 (3) (2011) 1675–1695, https://doi.org/10.1016/j.rser.2010.11.018.
[40] Z. Pavlík, J. Fořt, M. Pavlíková, J. Pokorný, A. Trník, R. Černý, Modified lime-cement plasters with enhanced thermal and hygric storage capacity for moderation of interior climate, Energy Build. 126 (2016) 113–127, https://doi.org/10.1016/j.enbuild.2016.05.004.
[41] M.I. Nizovtsev, A.N. Sterlyagov, Effect of phase change material (PCM) on thermal inertia of walls in lightweight buildings, J. Build. Eng. 82 (2024) 107912, https://doi.org/10.1016/j.jobe.2023.107912.
[42] F. Valentini, L. Fambri, A. Dorigato, A. Pegoretti, Production and characterization of TES-EPDM foams with paraffin for thermal management applications, Front. Mater. 8 (2021) 660656, https://doi.org/10.3389/fmats.2021.660656.
[43] F. Valentini, M. Grigiante, A. Prada, L. Fambri, A. Dorigato, A. Pegoretti, Experimental dynamic thermal properties determination of EPDM/NBR panels with a shape stabilized Phase Change Material based on summer daily temperatures of four cities in Italy, Energy Build. 318 (2024) 114503, https://doi.org/10.1016/j.enbuild.2024.114503.
[44] M. Mohan, V. Manjunath, S.M.Z. Mehdi, S.K. Soni, S.K. Dewangan, H. Lee, A. Awasthi, V.K. Sharma, A. Sharma, E. Song, N. Lee, J. Heo, K. Lee, B. Ahn, Phonon-photon synergy in phase change materials through nano-engineered carbon materials for multifunctional applications, Energy Storage Mater. 76 (2025) 104142, https://doi.org/10.1016/j.ensm.2025.104142.
[45] S. Sacchet, F. Valentini, A. Benin, M. Guidolin, R. Po, L. Fambri, Expanded graphite (EG) stabilization of stearic and palmitic acid mixture for thermal management of photovoltaic cells, C 10 (2) (2024), https://doi.org/10.3390/c10020046.
[46] S. Sacchet, F. Valentini, M. Guidolin, R. Po, L. Fambri, Shape-stabilized phase change materials with expanded graphite for thermal management of photovoltaic cells: selection of materials and preparation of panels, Appl. Sci. 15 (8) (2025), https://doi.org/10.3390/app15084352.
[47] S. Sacchet, F. Valentini, M. Coser, D. D'Amico, R. Po, L. Fambri, Efficacy of passive cooling panels for silicon photovoltaic mini-modules using phase change material and expanded graphite, Solar Energy Mater. Solar Cells 295 (2026) 113928, https://doi.org/10.1016/j.solmat.2025.113928.
[48] Z. Chen, X. Liu, C. Xin, F. Li, J. Lin, S. He, Flexible, robust, and leakage-resistant phase change composites: effect of the cross-linking network on performance, Energy Fuel 40 (9) (2026) 4864–4873, https://doi.org/10.1021/acs.energyfuels.5c06556.
[49] Z. Shi, Z. Liu, B. Quan, H. Yan, M. Sheng, C. Zhu, X. Yan, X. Hu, X. Lu, J. Qu, Enhancing light-to-thermal conversion performance of flexible EPDM/GNPs/PW phase change composites via salt-assisted EG exfoliation, Sol. Energy Mater. Sol. Cells 296 (2026) 114080, https://doi.org/10.1016/j.solmat.2025.114080.
[50] Z. Chen, Z. Chang, X. Li, W. Liu, J. Lin, L. Zhang, L. Chen, S. He, Surface energy matching and montmorillonite barriers enabled acrylonitrile butadiene rubber/palmitic acid phase change composites for high-performance thermal management, Polymer 350 (2026) 129776, https://doi.org/10.1016/j.polymer.2026.129776.
[51] D. Das, U. Bordoloi, H.H. Muigai, P. Kalita, A novel form stable PCM based bio composite material for solar thermal energy storage applications, J. Energy Storage 30 (2020) 101403, https://doi.org/10.1016/j.est.2020.101403.
[52] A.N.I.A. (ANIT), Materiali Isolanti e Conduttività termica. https://www.anit.it/wp-content/uploads/2021/03/IsolantiConduttivita_approfondimentoANIT_marzo2021.pdf.pdf, 2021.
[53] P.J. Shamberger, Cooling capacity figure of merit for phase change materials, J. Heat Transfer 138 (2) (2015) 024502, https://doi.org/10.1115/1.4031252.
[54] S. Sacchet, F. Valentini, C. Rizzo, R. Po, L. Fambri, High density polyethylene with phase change materials for thermal energy management, Energy Mater. 5 (4) (2025) 500042, https://doi.org/10.20517/energymater.2024.112.
[55] M.Q. Wu, S. Wu, Y.F. Cai, R.Z. Wang, T.X. Li, Form-stable phase change composites: preparation, performance, and applications for thermal energy conversion, storage and management, Energy Storage Mater. 42 (2021) 380–417, https://doi.org/10.1016/j.ensm.2021.07.019.
[56] M. Lachheb, Z. Younsi, N. Youssef, S. Bouadila, Enhancing building energy efficiency and thermal performance with PCM-Integrated brick walls: a comprehensive review, Build. Environ. 256 (2024) 111476, https://doi.org/10.1016/j.buildenv.2024.111476.
[57] X. Guo, H. Jiang, C.D. Qiu, T.H. Lu, R.Z. Wei, M.Z. Fan, Y. Zhang, W.S. Sun, An energy storage composite using cellulose grafted polyethylene glycol as solid-solid phase change material, Polym. Compos. 45 (2) (2024) 1524–1533, https://doi.org/10.1002/pc.27871.
[58] M. Li, X. Zhang, S. Zhou, Preparation and thermal/electrical properties of polypyrrole aerogel/diatomite-based anti-static phase change composite, Energy Build. 349 (2025) 116533, https://doi.org/10.1016/j.enbuild.2025.116533.
[59] M. Salimi, L.D. Nardo, V. Carvelli, Lightweight aggregates with shape-stabilized graphene and phase change material for energy storage concrete, Energy Build. 345 (2025) 116099, https://doi.org/10.1016/j.enbuild.2025.116099.
[60] Z. Nie, H. Zhang, Z. Lu, L. Zhou, J. Wang, S. Hu, J. Li, Y. Lu, Preparation of multifunctional silicone rubber composites with silver-coated phase change microcapsules for advanced thermal management, Compos. Sci. Technol. 262 (2025) 111052, https://doi.org/10.1016/j.compscitech.2025.111052.
[61] Y. Chen, S. Gao, C. Liu, Y. Situ, J. Liu, H. Huang, Preparation of PE-EPDM based phase change materials with great mechanical property, thermal conductivity and photo-thermal performance, Sol. Energy Mater. Sol. Cells 200 (2019) 109988, https://doi.org/10.1016/j.solmat.2019.109988.
[62] X. Hu, H. Wu, X. Lu, S. Liu, J. Qu, Improving thermal conductivity of ethylene propylene diene monomer/paraffin/expanded graphite shape-stabilized phase change materials with great thermal management potential via green steam explosion, Adv. Compos. Hybrid Mater. 4 (3) (2021) 478–491, https://doi.org/10.1007/s42114-021-00300-6.
[63] X. Hu, C. Zhu, H. Wu, X. Li, X. Lu, J. Qu, Large-scale preparation of flexible phase change composites with synergistically enhanced thermally conductive network for efficient low-grade thermal energy recovery and utilization, Compos. A: Appl. Sci. Manuf. 154 (2022) 106770, https://doi.org/10.1016/j.compositesa.2021.106770.
[64] Y. He, Y. Chen, C. Liu, L. Huang, C. Huang, J. Lu, H. Huang, Construction of three-dimensional network structure in polyethylene-EPDM-based phase change materials by carbon nanotube with enhanced thermal conductivity, mechanical property and photo-thermal conversion performance, Polymers. ISSN: 2073-4360 14 (2022) 11, https://doi.org/10.3390/polym14112285.
[65] M. Zhang, B. Quan, P. Chen, Y. Yang, C. Ding, S. Liu, H. Wu, X. Hu, X. Lu, Large-scale preparation of leakage-proof phase change composites with compressed enhanced thermally conductive network for efficient thermal management, J. Energy Storage 83 (2024) 110725, https://doi.org/10.1016/j.est.2024.110725.
[66] D. Mostofinejad, M. Abdoli, A. Saljoughian, A. Karimi, M. Eftekhar, Innovative energy-efficient lightweight concrete with improved thermal and mechanical properties using PCM-impregnated LECA aggregates, Construct. Build. Mater. 482 (2025) 141588, https://doi.org/10.1016/j.conbuildmat.2025.141588.
[67] A. El Majd, S. Sair, H.A. Ousaleh, K. Moulakhnif, Z. Younsi, N. Belouaggadia, A. El Bouari, Advanced gypsum/PCM composites incorporating biopolymer-encapsulated phase change materials for enhanced thermal management in buildings, Construct. Build. Mater. 451 (2024) 138872, https://doi.org/10.1016/j.conbuildmat.2024.138872.
[68] Y. Chen, C. Shi, X. Guo, C. Qing, D. Zou, A metal-based microencapsulated phase change material (MEPCM) with high thermal conductivity, electrical insulation and flame retardancy and its application in epoxy resin, Compos. A: Appl. Sci. Manuf. 180 (2024) 108081, https://doi.org/10.1016/j.compositesa.2024.108081.
[69] L. Spiridigliozzi, F. Valentini, S. Sacchet, M. Biesuz, A. Dorigato, S. Alcantara, G. Dell'Agli, Development of novel alkali-activated materials (AAMs) incorporating phase change materials (PCMs) for enhanced thermal regulation in sustainable buildings, J. Sustain. Cem.-Based Mater. (2026) 1–12, https://doi.org/10.1080/21650373.2026.2669201.
[70] C. Wang, C. Liu, C. Li, Additive manufacturing of shape-stabilized composite phase change materials via ultraviolet curing, Addit. Manuf. 61 (2023) 103341, https://doi.org/10.1016/j.addma.2022.103341.
[71] G. Fredi, E. Boso, A. Sorze, A. Pegoretti, Multifunctional sandwich composites with optimized phase change material content for simultaneous structural and thermal performance, Compos. A: Appl. Sci. Manuf. 186 (2024) 108382, https://doi.org/10.1016/j.compositesa.2024.108382.
[72] R. Vighnesh, V. Parol, K.B. Anand, Optimized parameters for novel shape stabilized PCM into porous vermiculite integrated in concrete roofings – a sustainable approach, Construct. Build. Mater. 490 (2025) 142566, https://doi.org/10.1016/j.conbuildmat.2025.142566.